

Charging effects in the inductively shunted Josephson junction

Jens Koch, V. Manucharyan, M. H. Devoret, and L. I. Glazman

Departments of Physics and Applied Physics, Yale University, New Haven, Connecticut 06520, USA

(Dated: November 1, 2018)

A Josephson junction shunted by a large inductance L supports two types of low-energy states, metaplasmon and persistent-current states. These are distinguished by their phase localization, level spacing, and magnetic flux dependence. We show that while the dynamical properties of a shunted junction approach those of the Cooper pair box, the inductive shunt removes the sensitivity to charge noise, and thus increases the prominence of charging effects.

PACS numbers: 85.25.Cp, 74.50.+r, 03.65.-w

Commonly, superconducting devices are divided into two categories: devices containing one or several superconducting islands, and devices devoid of such islands. The presence of islands, i.e. pieces of superconductor without any dc connection to ground, is associated with strong localization of charge and hence the manifestation of charging effects on the level of single Cooper pairs. This physics is utilized in both superconducting SETs [1] and Cooper pair boxes (CPBs) operating in the charge regime [2, 3]. One drawback of superconducting islands however, consists of their susceptibility to uncontrolled charge fluctuations in the environment. Such fluctuations hinders the control of devices via a gate electrode, and adversely affect their quantum coherence [4, 5]. Superconducting devices without islands, such as the rf SQUID [6], the single-junction flux qubit [7] and the phase qubit [8], are protected from the detrimental effects of charge noise. They typically operate in the regime of large intrinsic charge fluctuations and well-defined superconducting phase, $\langle \delta\varphi^2 \rangle \ll 2\pi$, where charging effects only play a subordinate role.

Despite the apparent intuition of this classification, there exist at least two counterexamples undermining the island-based distinction. Both the three-junction flux qubit [9] and the CPB in the transmon regime [10] possess superconducting islands but are insensitive to low-frequency charge noise due to large Josephson energy. Here, we demonstrate the existence of a third and complementary counterexample: a superconducting circuit which does not contain any islands, is insensitive to offset charges due to an inductive shunt, see Fig. 1 yet shows pronounced charging effects.

The origin of the reduced sensitivity to charge noise of the inductively shunted Josephson junction is identical to that of the rf SQUID, the single-junction flux qubit, and the flux-biased phase qubit [11], as the circuits of these devices are identical. Closing the Josephson junction by an inductive load allows one to evade the most severe problems caused by $1/f$ charge noise. Specifically, the vanishing dc impedance of the inductive element renders the energy spectrum independent of any constant offset charge, and transforms the $1/f$ charge noise into a relatively benign “ f -noise”. To confirm this, we start from the Hamiltonian belonging to the circuit of Fig. 1,

$$H = 4E_C(n - n_g)^2 - E_J \cos \varphi + \frac{1}{2}E_L(\varphi + 2\pi\Phi/\Phi_0)^2. \quad (1)$$

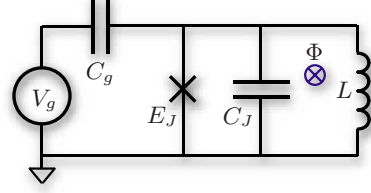


FIG. 1: Inductively shunted Josephson junction with charge bias. A superconducting inductance L shunts a Josephson junction with Josephson energy E_J and capacitance C_J . Offset charges and coherent drive is modeled by the capacitive coupling to a time-dependent gate voltage source $V_g(t)$. The magnetic flux through the superconducting loop is denoted as Φ .

Here, the canonically conjugate operators $n = q/2e$ and φ correspond to the junction capacitor charge (in units of Cooper pairs) and the superconducting phase difference across the junction, and they obey the relation $[\varphi, n] = i$. The three energy scales entering H are the (single-electron) charging energy $E_C = e^2/2(C_J + C_g)$, the Josephson energy E_J , and the inductive energy $E_L = (\Phi_0/2\pi)^2/L$, defined in terms of the flux quantum $\Phi_0 = h/2e$. The external magnetic flux through the loop is denoted by Φ , and the effect of the gate voltage is expressed in the offset charge $n_g = C_g V_g/2e + \delta n$, which additionally undergoes random fluctuations $\delta n(t)$ due to the dynamics of stray charges in the environment [5]. To analyze the effect of charge fluctuations, we apply a gauge transformation $\bar{\psi}(\varphi) = e^{in_g\varphi}\psi(\varphi)$. This results in a Hamiltonian \bar{H} , obtained from H by eliminating the offset charge n_g from the charging term and appending a term $-\hbar\dot{n}_g\varphi$. Thus, the energy spectrum only depends on the time derivative of the offset charge, in a fashion similar to the dependence on flux Φ , see Eq. (1) [16]. The relevant noise spectrum for \dot{n}_g is $S_{\dot{n}_g}(\omega) = \omega^2 S_{n_g}(\omega)$, such that Gaussian charge noise with a $1/f$ spectrum, $S_{n_g}(\omega) = A/|\omega|$ is transformed into benign “ f -noise”. Assuming an ultraviolet cutoff of the $1/f$ spectrum at frequency $1/\tau_u$, the residual effect of \dot{n}_g noise away from flux sweet spots and for long times $t \gg \tau_u$ is controlled by the behavior of the integral $f(t) = (\partial\omega_{ij}/\partial\dot{n}_g)^2 \int_{1/t}^{1/\tau_u} d\omega S_{n_g}(\omega)$, such that off-diagonal elements of the density matrix decay as $\rho_{ij} \sim \exp[-f(t)]$. For large t , the integral $f(t)$ is logarithmi-

cally divergent, yielding a slow power-law decay

$$\rho_{ij} \sim t^{-\frac{A}{\pi}} \left[\frac{\hbar\Phi_0}{2\pi E_L} \frac{\partial\omega_{ij}}{\partial\Phi} \right]^2, \quad (2)$$

where the exponent depends on the nature of the transition $i \rightarrow j$, and is much smaller for metaplasmon transitions than for transitions involving persistent-current states (see below). Equation (2) should be contrasted with the rapid loss of coherences in the absence of an inductive shunt, where $f(t)$ is replaced by $(\partial\omega_{ij}/\partial n_g)^2 t S_{n_g}(\omega=0)/2$, leading to an exponential decay with formally infinite coefficient.

In spite of the familiarity of the circuit in Fig. 1, its physics beyond the flux and phase qubit regimes ($E_C \ll E_L \lesssim E_J$) has remained largely unexplored, with the notable exception of the work by A. Kitaev [12]. Here, we examine the regime of large inductances where E_L represents the smallest energy scale, $E_L \ll E_C, E_J$. In practice, the main difficulty in realizing this new regime is the need for an inductive element with large inductance but small capacitance – an experimental challenge that has recently been shown to be surmountable by utilizing Josephson junction arrays [13]. Even though no islands are present in the circuit, we find that the structure of energy levels is related to the energy bands of the single-island CPB, and that certain dynamical properties approach those of the CPB in the limit of small E_L .

Yet, the small- E_L limit does *not* smoothly transform the energy spectrum of the inductively shunted device into that of the CPB. Ultimately, the reason for the subtlety of this limit stems from the opposed symmetries of the two systems: while the CPB has a strictly periodic potential when written in the phase basis, the inductive shunt always breaks this periodicity. Equivalently, the discrepancy may be formulated in the charge basis: due to the presence of an island in the CPB, charge on the corresponding node is quantized in terms of Cooper pairs, whereas the inductive shunt eliminates the island and renders the charge continuous. In the following, we study the small- E_L limit and support our findings with results from numerical diagonalization (employing the LC harmonic oscillator basis). Even though practical devices will operate at intermediate inductive energies away from this limit, an understanding of the small- E_L regime proves very useful as it enables an analytical treatment and elucidates the relevant physics.

The key to our analysis of the large-inductance limit consists of transforming the Hamiltonian (1) into the basis of Bloch waves $\{|s, p\rangle\}$, where $s \in \mathbb{N}$ is the band index and $p \in [0, 1)$ the quasimomentum. These states diagonalize the CPB part [comprising the terms $\sim E_C$ and E_J] of the Hamiltonian (1), $H_0 |s, p\rangle = \varepsilon_s(p) |s, p\rangle$, where the eigenenergies represent the usual CPB bands. For the transformation of the inductive term, we employ the standard relation $\varphi = id/dp + \Omega$ [14], where the Hermitian operator Ω causes interband coupling and is defined via

$$\langle ps|\Omega|p's'\rangle = \delta(p-p') \frac{i}{2\pi} \int_0^{2\pi} d\varphi u_{ps}^*(\varphi) \frac{du_{p's'}}{dp}(\varphi). \quad (3)$$

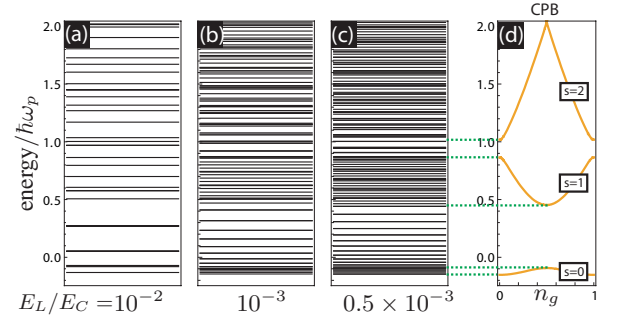


FIG. 2: (color online). Energy spectra for the inductively shunted Josephson junction at zero flux. The progression (a)–(c) shows energy spectra for $E_J/E_C = 2.5$ and decreasing inductive energy E_L . Energies are given in units of the plasma oscillation frequency $\hbar\omega_p = \sqrt{8E_J E_C}$. For small E_L , the spectrum exhibits regions with significantly different level spacings. (d) Comparison with the CPB bands for the same E_J/E_C ratio reveals that regions of small (large) level spacings coincide with band (gap) regions in the CPB.

Here, u_{ps} is the Bloch amplitude, $\langle\varphi|s, p\rangle = e^{ip\varphi} u_{s,p}(\varphi)$. The resulting form

$$H = \frac{E_L}{2} \left(\sum_{s,s'} |s'\rangle\langle s| \left[i\delta_{ss'} \frac{d}{dp} + \delta_{ss'} \frac{2\pi\Phi}{\Phi_0} + \Omega_{ss'}(p) \right] \right)^2 + \sum_s |s\rangle\langle s| \varepsilon_s(p), \quad (4)$$

describes a fictitious particle with inverse mass $\sim E_L$, and position p confined to a circle. The particle can assume different “flavors” corresponding to the band index s . The operator Ω induces interaction between flavors, which makes the problem nontrivial. However, for large E_J/E_C and low-lying bands s, s' we find $\Omega_{ss'}(p) \approx (2E_C/E_J)^{1/4} (\sqrt{s}\delta_{s,s'+1} + \sqrt{s'}\delta_{s,s'-1})/2\pi$ so that interband coupling can be neglected in this limit, simplifying the problem dramatically. The Hamiltonian becomes block-diagonal and separates into effective Hamiltonians

$$H^{(s)} = \frac{E_L}{2} \left(i \frac{d}{dp} + \frac{2\pi\Phi}{\Phi_0} \right)^2 + \varepsilon_s(p) \quad (5)$$

for the low-lying bands, whose spectra have to be overlaid. As a crucial insight, we note that Eq. (5) is structurally identical to the CPB Hamiltonian, and in the following we will draw from the knowledge of the CPB in both charge and transmon regimes [2, 15].

According to Eq. (5), E_L determines the kinetic energy while the CPB bands $\varepsilon_s(p)$ act as potentials for the inductively shunted device. The potentials are periodic and can be expressed as Fourier series $\varepsilon_s(p) = \sum_{\ell=0}^{\infty} \varepsilon_{s,\ell} \cos(2\pi\ell p)$, and approach simple sinusoids for large E_J/E_C . For small inductive energies, each low-lying CPB band supports two types of states: (i) *metaplasmon states* with approximate level spacing $2\pi\sqrt{E_L |\varepsilon_{s,1}|}$, which are bound states in the CPB potential, and are associated with large charge oscillation across the Josephson junction, and (ii) *persistent-current states*, existing

in the gaps of the “bare” ($E_L = 0$) CPB device; these states are associated with substantial persistent currents circulating (at finite E_L) through the inductor. As a result, the energy spectrum of the shunted junction separates into regions with distinctly different level spacings, where small (large) level spacing coincides with regions of bands (gaps) in the CPB, as illustrated in Fig. 2.

The nature of the persistent-current states can further be clarified by rewriting the Hamiltonian (5) in the discrete local-minimum basis $\{|m, s\rangle\}$, which formally parallels the charge basis of the CPB,

$$H^{(s)} = \frac{(2\pi)^2}{2} E_L (m + \Phi/\Phi_0)^2 + \frac{1}{2} \sum_{\ell=0}^{\infty} \sum_{m=-\infty}^{\infty} \varepsilon_{s,\ell} \left[|m, s\rangle \langle m + \ell, s| + \text{H.c.} \right]. \quad (6)$$

Physically, $|m, s\rangle$ corresponds to a state localized in the m -th local minimum of the phase-basis potential, carrying a persistent current $I_m^{(s)} = (m\Phi_0 + \Phi)/L$. From Eq. (6), the energies of persistent-current states are found to be

$$E_m^{(s)} \approx \varepsilon_{s,0} + 2\pi^2 E_L (m + \Phi/\Phi_0)^2, \quad (7)$$

where $m \in \mathbb{Z}$ has sufficiently large modulus so that $E_m^{(s)} > \max_p \varepsilon_s(p)$. Thus, to lowest order in the inter-well tunneling, the persistent-current states are doubly degenerate at zero flux, and each degenerate subspace is spanned by the two counter-propagating states with currents $I_{\pm m}^{(s)} \approx \pm m\Phi_0/L$ around the superconducting loop. At higher order in the inter-well tunneling, this degeneracy is lifted and time-reversal symmetry, which requires $I = 0$ for vanishing magnetic flux, is restored. The resulting avoided crossings are extremely small. Specifically, for a purely sinusoidal $s = 0$ band, i.e. $\varepsilon_{0,\ell} = 0$ for $\ell > 1$, the splitting between $|m, s = 0\rangle$ and $| -m, s = 0\rangle$ is generated by tunneling through the $2m$ potential barriers separating the two states, and scales as

$$\delta E_m \approx \varepsilon_{0,1} \left[\frac{\varepsilon_{0,1}}{(2\pi)^2 E_L} \right]^{2m-1} \frac{1}{[(2m-1)!]^2}. \quad (8)$$

Metaplasmon and persistent-current states also differ in their localization and respective flux dependence. As evident from Eq. (6) and illustrated in Fig. 3(a), metaplasmon states are typically delocalized across several wells around $\varphi = 0$, whereas persistent-current tend to localize in φ -space in the region of the corresponding parabolically deformed band. The flux dependence of these states is precisely analogous to the offset charge dependence of CPB levels in the transmon regime. For the bound metaplasmon states, the flux dependence is exponentially suppressed; specifically, variations in the metaplasmon states of band s scale as $\sim \exp[-4\sqrt{|\varepsilon_{s,0}|}/E_L/\pi]$. By contrast, Eq. (7) predicts that persistent-current states are strongly sensitive to magnetic flux. For the lowest bands, these predictions are confirmed by results from numerical diagonalization, see

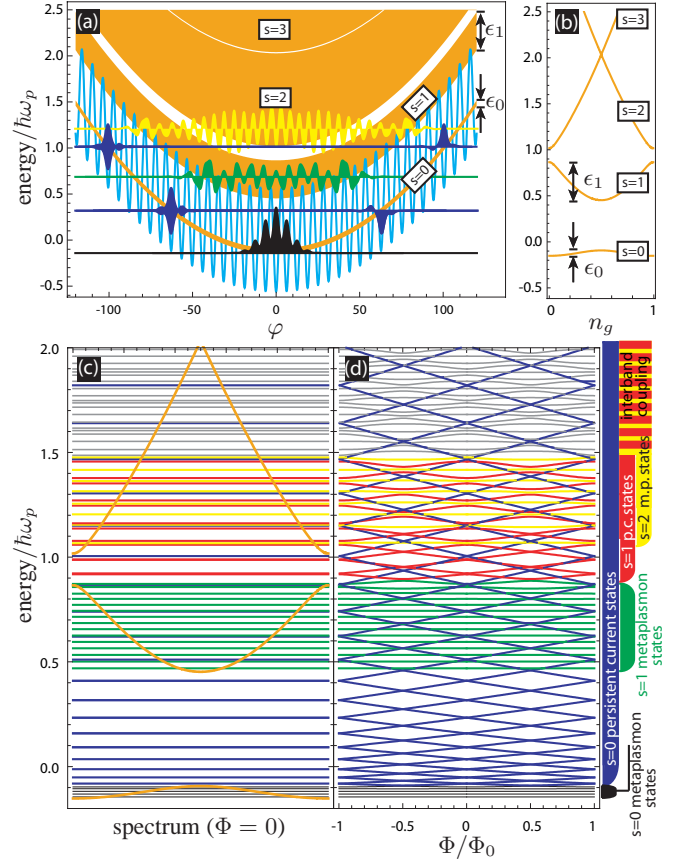


FIG. 3: (color). Metaplasmon and persistent-current states for large inductances. Panel (a) shows the potential in φ -space (cyan), the corresponding bent CPB bands (orange), and examples of wavefunctions at zero flux, from bottom to top: black–ground-state wavefunction (lowest $s=0$ metaplasmon state), blue– $s=0$ persistent-current states, green–lowest $s=1$ metaplasmon state, and yellow– $s=2$ metaplasmon state. Localization in φ -space differs characteristically, with metaplasmon states being centered at $\varphi = 0$ and delocalized, while persistent-current states are symmetric and antisymmetric superpositions of wavefunctions localized towards the edges of the parabolically deformed bands. (b) Corresponding CPB spectrum for comparison. Using the same color coding, (c) and (d) show the spectrum overlaid by the CPB bands, and the flux dependence of energy levels, respectively. Metaplasmon states (independent of flux) and persistent-current states (sensitive to flux) are easily distinguished. For the parameters chosen here, $E_J/E_C = 2.5$ and $E_L/E_C = 10^{-3}$, interband coupling becomes significant at higher energies (levels in gray), leading to avoided crossings between $s = 1$ persistent-current states (in red) and $s = 2$ metaplasmon states.

Fig. 3(d). Persistent-current states exist above the lowest CPB band and overlap with $s > 0$ metaplasmon states. At higher energies, avoided crossings between metaplasmon and persistent-current states become more significant, as interband coupling increases above the lowest bands.

The previous discussion underlines the differences between the spectra of the CPB and the inductively shunted Josephson junction: the presence of the inductor introduces new levels located in the band gaps of the CPB, and these levels do not

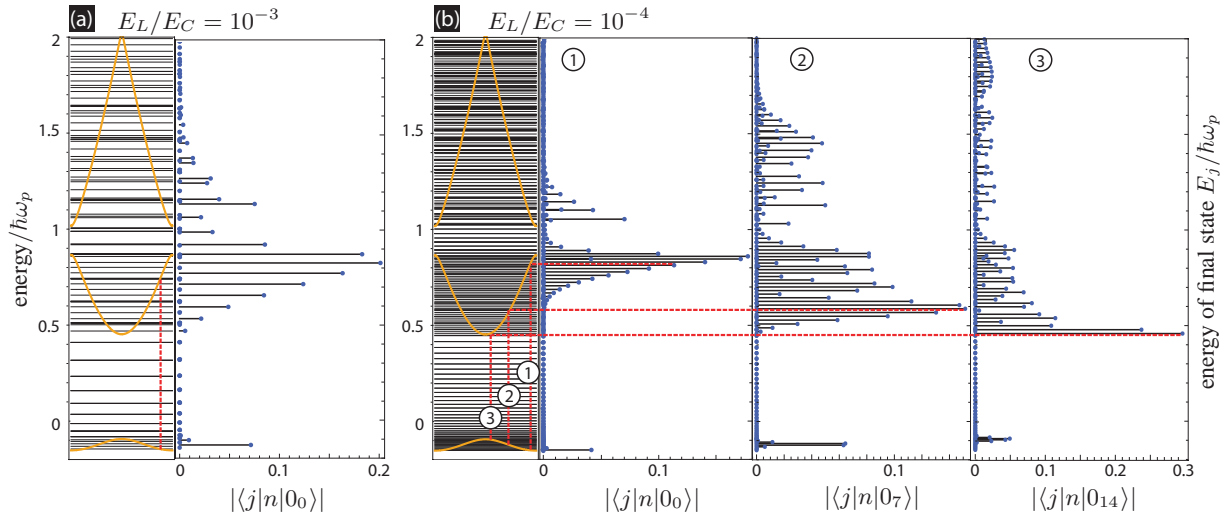


FIG. 4: (color online). Matrix elements relevant for excitation when coupling the junction charge to an ac voltage. The magnitude of the matrix element for a transition to final state $|j\rangle$ is shown as a function of the final state energy E_j , for several initial states. The prominent gap in the matrix elements demonstrates the strong suppression of transitions from metaplasmon states to persistent-current states. For transitions among metaplasmon states, the matrix element magnitude reaches a distinct maximum for the transition occurring in the corresponding CPB without the inductive shunt (vertical dashed lines). Lowering E_L makes the peak narrower, and eventually leads to a selection rule excluding all but the CPB-allowed transitions.

disappear in the limit of small E_L . However, we will now argue that in the limit of large inductance, the ac properties of the shunted device approach those of the CPB. To be specific, we consider the coupling the junction charge n to an ac voltage field, a scheme commonly used for control and readout of the CPB in the transmon regime [15]. Based on Eq. (1), the coupling term is obtained by adding an additional field term to the offset charge, $n_g \rightarrow n_g + C_g V_{\text{rms}}(a + a^\dagger)/2e$. Here, a , a^\dagger annihilate or create a photon in the microwave field mode, V_{rms} denotes its root-mean square voltage. Transitions are then induced by tuning the field into resonance, and the transition strength depends directly on the charge matrix elements $\langle f|n|i\rangle$, where i , f denote the initial and final states of the transition. At low energies where interband coupling is negligible, these states can be identified as eigenstates of Eq. (5), and we will write, e.g., $|i\rangle = |s_\nu\rangle$, thus denoting the ν -th eigenstate belonging to band s . We find

$$\begin{aligned} \langle s'_\nu | n | s_\nu \rangle &= i(E_J/2E_C)^{1/4} (\sqrt{s}\delta_{s,s'+1} - \sqrt{s'}\delta_{s,s'-1}) \\ &\times \int_{-1/2}^{1/2} dp \chi_{s'\nu'}^*(p) \chi_{s\nu}(p). \end{aligned} \quad (9)$$

The last integration involves the quasimomentum representation $\chi_{s\nu}(p) \equiv \langle sp | s_\nu \rangle$ of eigenstates, and is amenable to evaluation within the WKB approximation. In complete analogy to the Franck-Condon principle, the matrix elements peak when the transition between the corresponding classical turning points occurs vertically, see Fig. 4. For the metaplasmon transitions from $s = 0$ to 1 we find specifically that below the optimum the matrix elements decay exponentially with $\sim \exp[-\sqrt{2}|\varepsilon_{0,1}|E_L(\eta/|\varepsilon_{1,1}|)^{3/2}/2\pi]$, whereas for energies above, the decay is oscillatory and follows an overall

power-law decay $\sim [E_L^3/|\varepsilon_{11}\varepsilon_{01}|\eta]^{1/4}$, where η describes the energy deviation from the optimum. As a result, in the limit of large inductances the matrix elements select the CPB-allowed transitions, thus producing pronounced charging effects unimpeded by charge fluctuations.

To summarize, the physics of the inductively shunted Josephson junction in the large- L limit is distinct from the ones accessed by flux and phase qubits. Two different types of states, metaplasmon and persistent current states, with distinct level spacings and magnetic flux dependence dominate the spectrum at low energies. These findings have been successfully employed in the analysis of a recent experiment [13], and will be of future interest in exploring the device's applicability to quantum information processing and observation of Bloch oscillations.

We thank Alexei Kitaev for his talk at Yale, which exposed us to his work, and David Schuster, Göran Johansson, Robert Schoelkopf, and Steven Girvin for valuable discussions. This research was supported by the NSF under grants DMR-0754613, DMR-032-5580, the NSA through ARO Grant No. W911NF-05-01-0365, the Keck foundation, and Agence Nationale pour la Recherche under grant ANR07-CEXC-003. M.H.D. acknowledges partial support from College de France.

-
- [1] D. V. Averin et al., Phys. Rev. Lett. **78**, 4821 (1997).
 - [2] V. Bouchiat et al., Physica Scripta **T76**, 165 (1998).
 - [3] Y. Nakamura, Y. A. Pashkin, and J. S. Tsai, Nature (London) **398**, 786 (1999).
 - [4] G. Zimmerli et al., Appl. Phys. Lett. **61**, 237 (1992).

- [5] A. B. Zorin et al., Phys. Rev. B **53**, 13682 (1996).
- [6] A. Barone and G. Paterno, *Physics and Applications of the Josephson Effect* (John Wiley and Sons, 1982).
- [7] J. R. Friedman et al., Nature (London) **406**, 43 (2000).
- [8] J. M. Martinis et al., Phys. Rev. Lett. **89**, 117901 (2002).
- [9] C. H. van der Wal et al., Science **290**, 773 (2000).
- [10] J. A. Schreier et al., Phys. Rev. B **77**, 180502(R) (2008).
- [11] R. Simmonds et al., Phys. Rev. Lett. **93**, 077003 (2004).
- [12] A. Kitaev, unpublished work presented in a talk at Yale University (2008).
- [13] V. Manucharyan et al., in preparation (2009).
- [14] E. M. Lifshitz and L. P. Pitaevskii, *Statistical Physics, Part 2*, Chapter 6 (Butterworth-Heinemann, 1980).
- [15] J. Koch et al., Phys. Rev. A **76**, 042319 (2007).
- [16] We emphasize that this reasoning does *not* apply to the Cooper pair box, where the gauge transformation additionally affects the quasi-periodic boundary conditions.